ELSEVIER

Journal of Electron Spectroscopy and Related Phenomena 114–116 (2001) 855–863

JOURNAL OF ELECTRON SPECTROSCOPY and Related Phenomena

www.elsevier.nl/locate/elspec

L-edge X-ray absorption spectroscopy of some Ni enzymes: probe of Ni electronic structure

Hongxin Wang[a,b], Daulat S. Patil[b], Weiwei Gu[a], Lilian Jacquamet[a], Stephan Friedrich[b,c], Tobias Funk[b], Stephen P. Cramer[a,b,*]

[a]*Department of Applied Science, University of California, Davis, CA 95616, USA*
[b]*Lawrence Berkeley National Laboratory, Berkeley, CA 94720, USA*
[c]*Lawrence Livermore National Laboratory, Livermore, CA 94551, USA*

Received 8 August 2000; received in revised form 3 October 2000; accepted 3 October 2000

Abstract

L-edge X-ray absorption spectroscopy has been used to study the electronic structure of Ni in the Ni–Fe hydrogenases and CO-dehydrogenases under a variety of conditions. The L-edge spectra are interpreted by comparison with the spectra of Ni model complexes and by ligand field multiplet simulations to examine the Ni oxidation and electronic spin states. The spectra for Ni in oxidized *Desulfovibrio gigas* and *Pyrococcus furiosus* enzymes are consistent with a covalent Ni^{III} species. All of the reduced hydrogenases in this study exhibit a high spin Ni^{II} spectrum, and no Ni^{I} has been observed. In contrast to hydrogenases, the native *Clostridium thermoaceticum* CO-dehydrogenase has a low spin Ni^{II} and exhibits a clearly different spectral multiplet. Spectroscopy of Ni enzymes using a 15-eV resolution STJ detector and using the new ALS beamline 4.0.2 with a 0.2 eV energy resolution show great promises for future biological L-edge spectroscopy. © 2001 Elsevier Science B.V. All rights reserved.

Keywords: Ni enzymes; Ni L-edges; Hydrogenase; CO-dehydrogenase; Superconducting tunneling junction detector

1. Introduction

The variety of nickel oxidation states (from −1 to +4) and local geometry (octahedral, tetrahedral, tetragonal, trigonal bi-pyramidal and square planar, etc.) makes Ni complexes important in coordination chemistry. In biology, Ni is an essential trace element in a large variety of enzymes, such as Ni–Fe hydrogenase, CO-dehydrogenase, urease and methyl-coenzyme–M reductase [1]. Ni–Fe hydrogenases [2,3] have an unusual Ni–Fe center, which is catalytically active, and two/three of Fe–S clusters for electron transfer (see Fig. 1, top inset). The as-isolated *Desulfovibrio gigas* hydrogenase exhibits two EPR active (S=1/2) states: Ni–A and a small amount of Ni–B. Activation with hydrogen puts the Ni in a manifold of three active species: the EPR silent Ni–SI, EPR detectable Ni–C and another EPR silent Ni–R [4]. The oxidation states of Ni in these states have been the subject of numerous proposals, including Ni^{III}–Ni^{II}– Ni^{I}– Ni^{0} [5], Ni^{III}–Ni^{II}– Ni^{I}–Ni^{I} [6], Ni^{III}–Ni^{II}– Ni^{III}– Ni^{II} [7], and ligand based redox reactions [8]. CO incubation following the H_2 activation leads to a CO-inhibited and non-active state, which we call Ni–CO. Chemical (e.g. dithionite) reduction puts Ni–A/B in a reduced but 'un-

*Corresponding author.

0368-2048/01/$ – see front matter © 2001 Elsevier Science B.V. All rights reserved.
PII: S0368-2048(00)00370-4

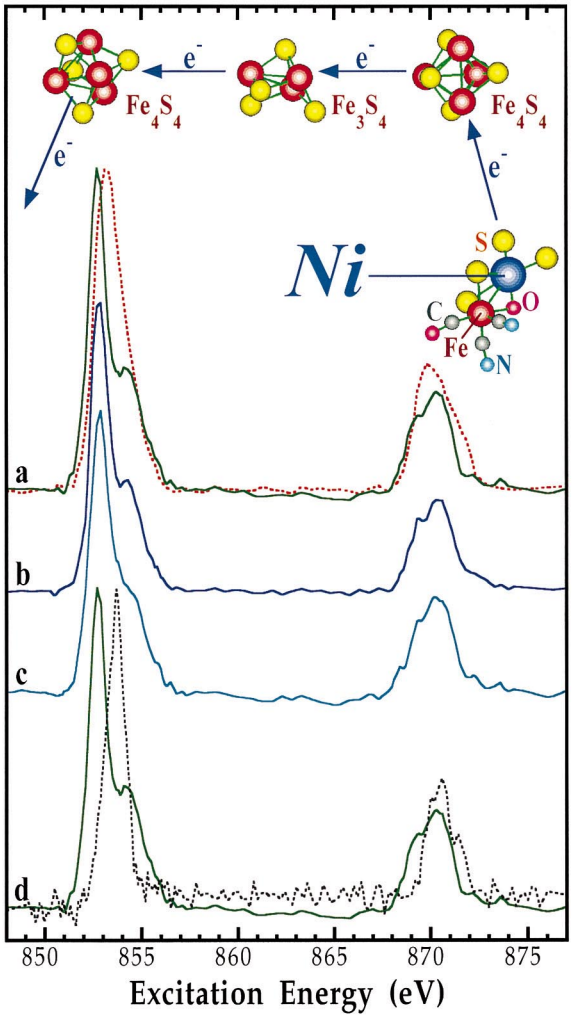

Fig. 1. L-edge absorption spectra of *D. gigas* hydrogenase. The spectra are for (a) as-isolated (dashed line) versus H_2 reduced (solid line) forms; (b) dithionite reduced form; (c) CO treated form and (d) H_2 reduced *D. gigas* hydrogenase (solid line) versus the native Ct-CODH (dashed line). The top inset is a picture showing the major metal clusters inside as-isolated *D. gigas* hydrogenase.

ready' state – Ni–SU [4]. Unresolved oxidation states have contributed to many longstanding controversies in the catalytic mechanism of this enzyme, such as whether Ni is redox active. Other hydrogenases (e.g. it and *Pyrococcus furiosus* hydrogenases) and other Ni enzymes also have the same problem. Study of electronic spin state, on the other hand, is important both in aiding the assignment of oxidation states and in understanding spin coupling properties.The L-edge X-ray absorption spectroscopy (XAS) is one of the best tools for studying electronic structure of the first row (3d) transition metals [9]. First, XAS is element (Ni) specific in comparison with conventional methods, such as EPR, FTIR or UV-visible spectroscopy. Second, L-edges have several advantages over K-edges, for example a 3–5 times better energy resolution, a dipole-allowed transition (2p→3d), and a calculable spectral multiplet [9,10], which is often diagnostic of the ligand binding orbitals. In this paper, the L-edge absorption spectroscopy for Ni–Fe hydrogenases has been studied to illustrate its excellent ability in resolving the Ni enzyme's oxidation states and spin states. We also report a high resolution fluorescence spectrum of as-isolated *D. gigas* hydrogenase using a 15-eV resolution superconducting tunneling junction detector and a preliminary spectrum for Ni azurin collected by using the new ALS beamline 4.0.2. These results show great promise for future biological L-edge spectroscopy.

2. Experimental section

2.1. XAS Measurement and analysis

Although L-edge absorption spectroscopy is well known in solid state and surface science, its biological application has been hindered by some technical difficulties associated with biological samples in UHV chamber and their dilute metal concentration [11]. Progress has been made over the past decade in this area [11,12] and including procedures to make partially dehydrated samples with biological activities, and to extract the weak metal fluorescence signal using a Ge detector. The experimental setup for this study was the same as previously reported [12]. The measurement was done inside a UHV chamber (5×10^{-9} Torr) under windowless operation. L-edge spectra of model compounds were recorded by total electron yield with a channeltron and Ni enzymes were measured by X-ray fluorescence with a 13-element or a 30-element Ge detector. One integration region was defined around the Ni L fluorescence signal (F) while the second window was set around the O K fluorescence, used as a measure of the incident intensity (I_0). The

incident beam intensity was also independently monitored by the photocurrent measurement from a gold-coated grid in front of the samples. The raw spectrum (F/I_0) was then collected as a function of excitation energy. Each model spectrum is the sum of three 15-min scans while each protein spectrum represents the sum of approximately 40 20-min scans. The spectra were calibrated hourly with NiF_2, using its absorption maximum at 852.7 eV [13]. To minimize radiation damage, the position of the X-ray beam on the sample was moved every few scans. No change was observed in the spectra over time. The experiments were performed at Stanford Synchrotron Radiation Laboratory (SSRL) beamline 8–2 [14] and at Advanced Light Source (ALS) beamline 9.3.2 [15] and 4.0.2. Their energy resolutions are 1.0 eV, 0.4 eV and 0.2 eV respectively. The L-edge data were analyzed as reported [9,11]. A correlation diagram of L_3 absorption centroid versus branching ratio was developed to separate nickel with different electronic structures. The branching ratio is defined as $L_2/(L_2+L_3)$, where L_i ($i=2,3$) is the integrated intensity for the observed L_i peak. Theoretical simulations of L-edge spectra were calculated for Ni^{I}, Ni^{II}, and Ni^{III} using published methods [9,10]. The ab initio Hartree–Fock values of the Slater integrals and spin–orbit couplings (ξ_{2p} and ξ_{3d}) were used as tabulated. Charge transfer effects were taken into account by a reduction of the Slater integrals in the calculation. Ligand field parameters $10D_q$, D_s and D_t were adjusted to yield a good match between calculated and experimental spectra.

2.2. Sample preparation and transfer

The sample preparation procedure is as reported before [16,17]. Partially dehydrated films for L-edge experiments were prepared by syringing a drop (~10–20 μl) of protein solution onto a silicon wafer or a sapphire square and allowing it to dry under the appropriate atmosphere (N_2, H_2 or CO). The enzyme samples prepared in this study were: (1) as-isolated, H_2 reduced, dithionite reduced and H_2 reduced followed by CO incubation (referred as CO treated) *Desulfovibrio gigas* hydrogenase; (2) oxidized and H_2 reduced *Paracoccus furiosus* hydrogenase; and (3) as-isolated *Clostridium thermoaceticum* CO-dehydrogenase (Ct-CODH). The FTIR spectra were recorded to monitor the states of these samples [16]. The samples were transferred anaerobically using a loadlock onto the cold finger maintained with liquid helium flow (inside the UHV chamber). To alleviate the concerns that samples might undergo alternation when the 'bare' protein films are exposed to vacuum, additional protein spectra were recorded on 'sealed' or 'capped' samples. In the case of the 'sealed' samples, the samples were sealed behind a 5000 Å silicon nitride membrane before and throughout the X-ray measurement. In 'capped' samples, the sapphire plate with Ni enzyme film was mounted onto a gold plated copper support and sealed with a cap under N_2, H_2 or CO atmosphere. The cell was then transferred through a loadlock into the vacuum chamber and threaded onto a liquid helium cooled cold finger. After ~30 min, the cap was unthreaded and the X-ray experiments commenced. The spectra for 'window-sealed' and 'capped' samples were recorded at SSRL beamline 8–2 with 1.0–1.4 eV energy resolution.

3. Results and discussions

3.1. Hydrogenase overview – Ni^{III} vs. Ni^{II}

We begin by illustrating the general similarity of L-edges for reduced (H_2 reduced, dithionite reduced and CO treated) *D. gigas* hydrogenase, as well as the clear differences observed between reduced and oxidized forms (Fig. 1). The as-isolated *D. gigas* hydrogenase spectrum (a, dashed line) has a broad L_3 maximum near 853.5 eV and a relatively sharp L_2 edge, while H_2 reduced enzyme (a, solid line) has a primary L_3 peak near 853.2 eV, along with a weaker and broader L_2 edge. The L_3 centroid shifts from 854.0 eV as in as-isolated form to 853.35 eV as in H_2 reduced state. The dithionite reduced (b) and CO treated (c) spectra have L_3 centroids at 853.6 eV and 853.5 eV and branching ratios at 0.76 and 0.75 respectively, similar with H_2 reduced hydrogenase spectrum.

Soft X-ray L-edge spectroscopy is still a relatively novel technique for probing bioinorganic samples. For this reason, we illustrate some effects of oxidation states, spin states, and covalency, using the model complexes reported in our recent publications

[16,17]. As shown in Fig. 2 left, the average L_3 absorption centroid shifts to higher energy position as Ni was oxidized from Ni^{I} to Ni^{II}, Ni^{III} and Ni^{IV}. Another important feature of L-edges is that the strong interactions between core hole and 3d orbitals give rise to the 'multiplet structure'. Of particular relevance to Ni enzymes (see Fig. 2, left): (1) Ni^{I} spectra do not exhibit multiplet structure because the d-shell is full in the final state; (2) High-spin (hs) Ni^{II} spectra and low-spin (ls) Ni^{II} spectra have clearly different spectral multiplets, which will be addressed in details later; (3) ionic Ni^{III} multiplet features occur on the low energy side of the L_3 peak, while covalent Ni^{III} spectra have broad peaks without clear multiplet structure. Finally, Ni in $KNiIO_6$ represents the most oxidized Ni form that we have encountered and appears to be a true Ni^{IV} [18].

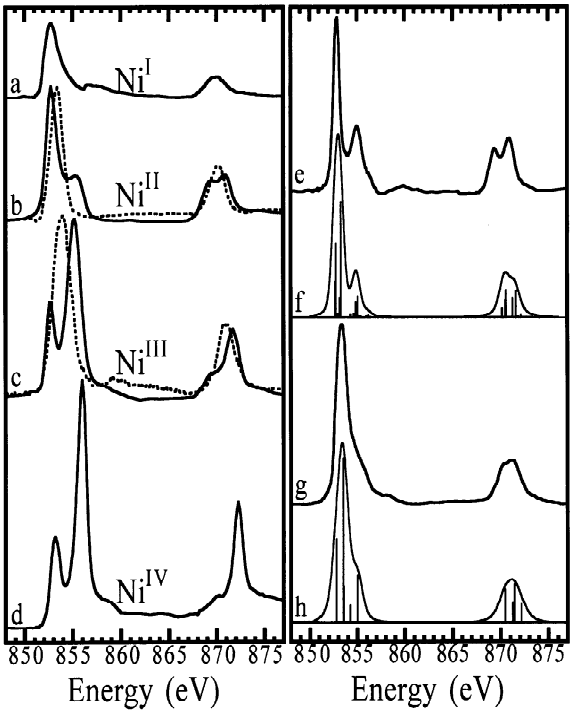

Fig. 2. In the left panel: examples of L-edge spectra of some model Ni complexes [16]. (a) Ni^{I}: Ni^{I}"S_4"; (b). high spin Ni^{II} (solid line, Ni doped MgO) versus low spin Ni^{II} (dashed line, Ni^{II}"S_4"); (c). ionic Ni^{III} (solid line, $Li[Ni^{III}(\kappa^4\text{-mac*})]$) versus covalent Ni^{III} (dashed line, $[Ni^{III}(pdtc_2)]^-$); (d). Ni^{IV}: $KNi^{IV}IO_6$. In the right panel: (e) the high spin Ni doped MgO; (f) ligand field simulation assuming a D_{4h} Ni symmetry; (g) high spin $Ni^{II}(DAPA)Cl_2$ and (h) a simulation with a D_{3h} symmetry.

Unlike ionic Ni^{III} complexes (such as $K_3Ni^{III}F_6$), the multiplet structure for more covalent Ni^{III} complexes, such as those with sulfur donor ligands, is unresolved and the L_3 absorption centroid moves ~0.5 eV lower to ~854 eV [16]. These complexes clearly have a significant amount of Ni^{II}-ligand hole character. With the combination of L_3 centroid and spectral feature, we simply note that the as-isolated *D. gigas* hydrogenase L-edges (Fig. 1a, dashed line) strongly resemble spectra for Ni^{III} model compounds with sulfur donors, such as $[Ni^{III}pdtc_2]^-$. On the other hand, the spectra for H_2 (Fig. 1a) and dithionite (Fig. 1b) reduced *D. gigas* hydrogenase both show a resolved secondary peak on the high energy side of the L_3 maximum and a broad L_2 peak, resembling the ionic hs-Ni^{II} complex-Ni doped MgO (Fig. 2e). These spectra are reproducible by ligand field simulation with a D_{4h} Ni orbital symmetry (Fig. 2f). The CO treated *D. gigas* hydrogenase (Fig. 1c) has a shoulder instead of a resolved peak on the higher energy side of the main L_3 peak and is similar with the spectra of more covalent high-spin Ni^{II} complexes (*e.g.* $Ni^{II}(DAPA)Cl_2$, Fig. 2g). However, caution must be excised in determining whether these enzymes have an ionic or a covalent Ni^{II} because, for instance, such a partially resolved hs-Ni^{II} can be well simulated assuming a different (D_{3h}) Ni symmetry (Fig. 2h). Nevertheless, there is little doubt that the reduced nickel probed here are hs-Ni^{II}. No evidence of Ni^{I} has been observed in any reduced hydrogenase spectra.

3.2. Correlation diagram and sum rule analysis

Since some L-edge spectra have no observable multiplet structure, other characteristics of the spectra must be exploited. The combination of L_3 centroid and branching ratio (Fig. 3) allows the segregation of Ni complexes into different regions: (1) The average centroids differ by nearly 1 eV per oxidation state – 852.55 eV for Ni^{I} and 853.4/843.5 eV for hs-/ls-Ni^{II} and 854.5 for Ni^{III} on our calibration scale; (2) The branching ratio changes with spin state [19]. The low spin complexes have branching ratios ranging from 0.63 to 0.70, with an average of 0.67, while high spin complexes ranged from 0.71 to 0.77, with an average of 0.74; (3) The high spin Ni^{III}

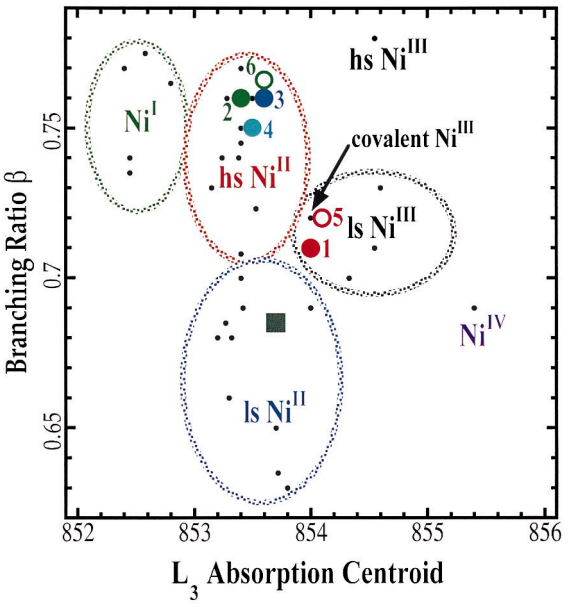

Fig. 3. Correlation diagram of L_3 absorption centroid versus branching ratio for various Ni models with known oxidation and spin states [17]. The Ni complexes are segregated as Ni^{I}, high spin Ni^{II}, low spin Ni^{II} and Ni^{III} regions. Small dots are the Ni model data [17] and the dashed circles are the eye-guides only. The filled circles are as-isolated (red, 1), H_2 (green, 2), dithionite (blue, 3) reduced and CO treated (light blue, 4) *D. gigas* hydrogenase. The open circles are oxidized (red, 5) and H_2 reduced (green, 6) *P. furiosus* hydrogenase. The filled square (gray) is the low spin as-isolated Ct-CODH.

complex K_3NiF_6 has a similar L_3 centroid with but a significant higher branching ratio than other Ni^{III} complexes; (4) Formally Ni^{III} complex $[Ni^{III}pdtc_2]^-$ has a L_3 centroid at 854.0 eV which is close to some low-spin Ni^{II} (Fig. 3), indicating a significant fraction of ligand oxidation.

The L_3 centroids for oxidized *D. gigas* and *P. furiosus* hydrogenases are located in the junction region of Ni^{II} and Ni^{III}, consistent with a covalent Ni^{III}. However, without additional evidence they could also be interpreted as a Ni^{II} species in a more ionic environment. All the reduced forms are located in the high spin Ni^{II} region, again disfavoring a Ni^{I} center. For Ni^{II} and Ni^{III} complexes with the same ligand, typical shifts are ~1 eV for ionic complexes such as $[Ni^{II,\,III}(cyclam)]^{2+/3+}$ and 0.6 eV for covalent species such as $[Ni^{II,\,III}(pdtc_2)]^{2-/-}$ [20]. The L_3 absorption maximum for Ni^{II} compounds generally range from 853.2 to 853.9 eV. Thus, the changes observed between the as-isolated (854.0 eV) and the reduced (853.35 eV) *D. gigas* hydrogenase spectra are consistent with the reduction of a covalent Ni^{III} complex to a Ni^{II} species [21]. The reduced/oxidized *P. furiosus* hydrogenase L-edge spectra (not shown), L_3 centroids and branching ratios (Fig. 3) resemble those for the corresponding *D. gigas* hydrogenase, also consistent with a $Ni^{III} \rightarrow Ni^{II}$ reduction.

A final useful property of L-edge spectra, which results from the X-ray ''sum rule'' [18,22], is the normalized integrated intensity of the $2p \rightarrow 3d$ transitions. Since d^7 Ni^{III} has formally one and half times the number of *d*-vacancies as d^8 Ni^{II}, the L_3 and L_2 integrated intensity should have the same ratio between Ni^{III} and Ni^{II} species. As shown in Fig. 4 (top inset) the integrated L intensity for a series of Ni models did exhibit a nice linear correlation with oxidation state, after being normalized to the non-resonance edge jump [18]. Unfortunately Ni enzyme spectra do not have a clear continuum step required for spectral normalization [18], therefore other normalization standards must be used. For this purpose,

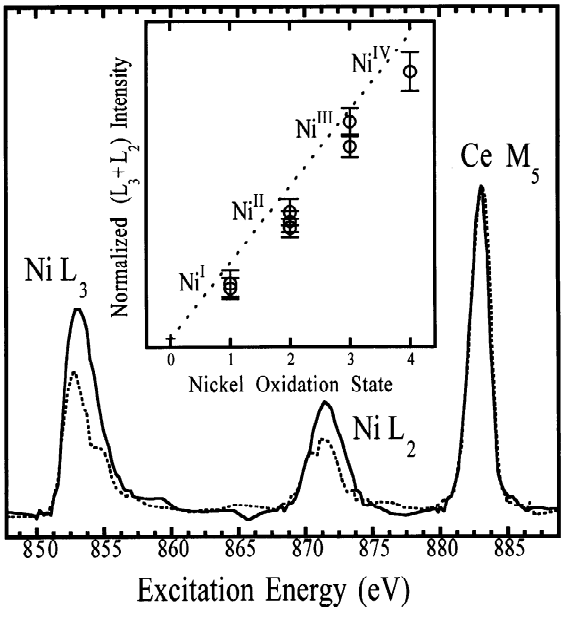

Fig. 4. Ni L-edge spectra of cerium doped, as-isolated (dashed line) and H_2 reduced (solid line) *D. gigas* hydrogenase. The top inset shows the Ni model integrated intensities versus the number of 3d holes [18].

the element cerium (Ce) was chosen for its M_5 absorption edge in the energy region comparable to Ni L-edge. Experimentally, we added the exactly same amount of redox insensitive cerium nitrate into both as-isolated and H_2 reduced *D. gigas* hydrogenase.

The Ni L-edge spectra were normalized to the intensity of Ce M_5-edge at ~884 eV, as shown in Fig. 4. Ce M_5-edge absorption can also be used as an internal energy calibration standard once it is calibrated with NiF_2. The Ni L-edge integrated intensities were calculated as 0.92 for as-isolated and 0.66 for H_2 reduced samples, and normalized to the integrated Ce–M_5 intensity (0.58). After normalization, the ratio of the Ni $L_{2,3}$ integrated intensities for as-isolated and H_2 reduced forms was derived as 1.39, consistent with a $Ni^{III} \rightarrow Ni^{II}$ reduction suggested by our L-edge multiplet and by most of the previous K-edge results [21]. However, this preliminary result only illustrates good feasibility for sum rule analysis, more careful study is necessary to draw any quantitative conclusions.

3.3. High spin vs. low spin Ni^{II}

As shown in Fig. 2, the hs-Ni^{II} and the ls-Ni^{II} complexes have distinctly different spectral features. The hs-Ni^{II} spectra have multiplet structure on the high energy side of the L_3 maximum and broader or split L_2-edges while ls-Ni^{II} spectra have little multiplet on the L_3 peak and relatively sharper and strong L_2-edges [23]. The L_3 absorption maximum generally appears at higher energy for low spin than for high-spin complexes, presumably because the single remaining vacant orbital has been raised to a relatively higher energy by the ligand field. In the correlation diagram (Fig. 3), hs-Ni^{II} spectra have much higher branching ratios than ls-Ni^{II} spectra.

From the facts of secondary structures on the high energy side of the main L_3 peak, broader L_2-edges (Fig. 1) and high branching ratios (Fig. 3), all the reduced hydrogenase clearly have a high spin Ni^{II} center. Although our argument for high-spin Ni^{II} in the reduced hydrogenases is at odds with the previous low spin Ni^{II} assignment [2,21,24,25], an octahedral complex with two hydride ligands, or a trigonal pyramidal (five coordinate) complex with a single hydride [26,27] would be consistent with high-spin Ni^{II}. In this study, the reduced hydrogenases were all sealed with either a silicon nitride window or a cap during L-edge measurement so that the concern of sample alternation in vacuum is alleviated. A recent publication [16] contains a detailed discussion of every piece of evidence and the overall evaluation.

The differences between high spin and low spin Ni^{II} are clear for various Ni models, however, it is useful to see a comparison between different Ni enzymes. We thus have examined the L-edge spectrum for a more square planar and low spin Ni^{II} site [28,29] inside as-isolated *C. thermoaceticum* CO-dehydrogenase (Ct-CODH). Ct-CODH is another kind of Ni enzyme which catalyzes CO oxidation and acetyl-CoA synthesis [17,29]. As shown in Fig. 1(d), the five or six coordinated [21,27] Ni in hydrogenase (form R of *D. gigas*, solid line) has a high spin Ni^{II} spectrum. In contrast, the more square planar Ni site in Ct-CODH (dashed line) exhibits an L-edge feature of low spin Ni^{II}, including: (1). absence of spectral multiplet in both L_3 and L_2; (2). a higher L_3 maximum (853.7 eV) than the high-spin *D. gigas* hydrogenase (853.4 eV); and (3). a clearly lower branching ratio (Fig. 3, filled square). From the comparison, there is little doubt that the reduced hydrogenases have a high spin Ni^{II} while the native Ct-CODH has a low spin Ni^{II}.

3.4. New research directions

One of the difficulties in biological L-edge X-ray spectroscopy is the dilute metal signal in biological samples combined with a huge background of oxygen fluorescence [12]. A Ge detector has a practical energy resolution of ~200 eV. Although Ni L-edge fluorescence (853 eV) is more than 300 eV higher than the O K fluorescence (525 eV), the huge difference in their amplitudes makes Ni barely resolvable from the huge O K fluorescence peak. This certainly limits the signal-to-noise ratio for our experiment. Superconducting tunnel junctions (STJs) can be used as high-resolution energy-dispersive X-ray detectors. STJ detectors are based on the measurement of an increased tunneling current from excess charge carriers that are excited above the

superconducting energy gap by the absorption of an X-ray photon. Nb-based STJ detectors have a theoretical energy resolution limit below 5 eV FWHM for X-ray energies up to 1 keV at count rates up to 10,000 counts/s. We recently used the newly developed Nb-Al-AlOx-Al-Nb X-ray detectors and recorded an L-edge X-ray fluorescence spectrum for as-isolated *D. gigas* hydrogenase (Fig. 5). In this particular experiment, the detector resolution is 15 eV FWHM at O K-edge (525 eV) [30]. Earlier experiments with smaller STJ detectors have shown an even higher resolution of 1.7–8.9 eV for photon energy between 50 and 1000 eV [31]. As seen in Fig. 5 [30], Ni L-edge fluorescence signal is clearly resolved from the huge O K fluorescence peak (1.3×10^6 counts/s) and, therefore, the Ni-windowed absorption spectra should have much less noise if a STJ detector is used in the future. Fig. 5 (top inset) also illustrates the newest 3×3 STJ detector array which is being developed in collaboration with Lawrence Livermore National Laboratory.

On the other hand, the development of undulator beamlines in the third-generation synchrotron radiation, such as the new ALS beamline 4.0.2, provides us with several orders of magnitude higher X-ray beam intensity. Besides the higher flux, on these beamlines it is easier to achieve energy resolution than traditional bend magnet beamlines, such as the SSRL 8–2. Fig. 6 (panel I–IV) illustrates an array of 3d metal complexes measured recently the new ALS beamline 4.0.2, with an energy resolution of 0.2 eV at ~850 eV. All these model compound spectra show well-resolved multiplet features, exhibiting the excellent capability of this beamline. Panel V on the right side is a preliminary Ni protein (Ni azurin) spectrum obtained in this beamline with one scan. Also in the right panel are the NiF_2 spectra measured at this beamline (b) and at SSRL beamline 8-2 (c).

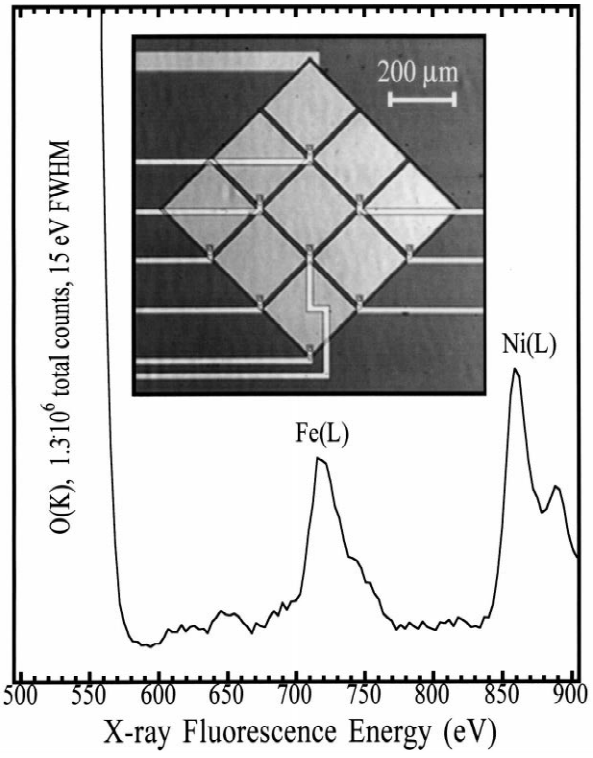

Fig. 5. Ni L-edge Fluorescence spectrum of as-isolated *D. gigas* hydrogenase taken with a superconducting tunneling junction (STJ) detector [30]. The top inset is the photo of a new 3×3 STJ detector array.

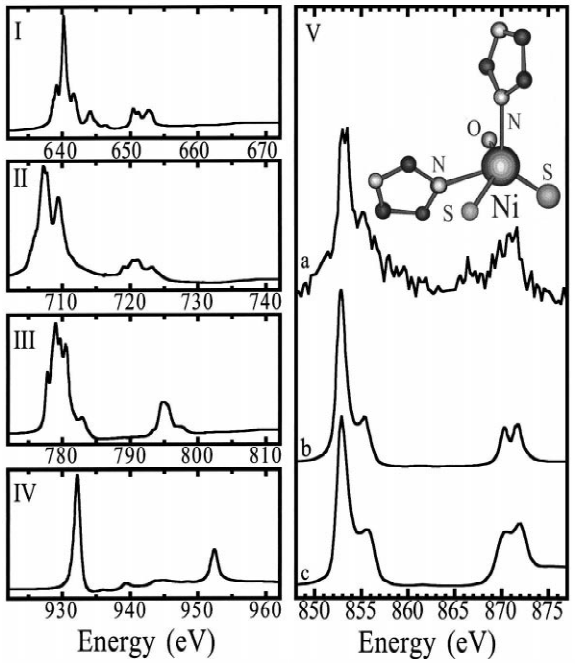

Fig. 6. In the left panel: (I–IV) the L-edge spectra of 3d transition metal complexes recorded on new ALS beamline 4.0.2: (I) MnF_2; (II) FeF_2; (III) CoF_2; (IV) $CuCl_2$. In the right panel (V): (a) preliminary spectrum of Ni azurin measured in beamline 4.0.2; (b) the NiF_2 spectrum taken at ALS 4.0.2; and (c) the NiF_2 spectrum recorded at SSRL beamline 8-2.

4. Summary

In this paper, L-edge spectra for Ni–Fe hydrogenases and CO-dehydrogenase have been studied. The L-edge spectra are interpreted by comparison both with model compound spectra and with the theoretical ligand field simulations. The clear spectral differences between the different enzymatic nickels illustrate the ability of the L-edge absorption spectroscopy to resolve oxidation and electronic spin states. The feasibility of sum rule analysis on dilute Ni enzyme samples has also been tested. Our L-edge results show that oxidized *D. gigas* and *P. furiosus* hydrogenases are consistent with a covalent Ni^{III} species while all of the reduced enzyme samples in this study show a high spin Ni^{II} multiplet. No Ni^{I} has been observed in Ni–Fe hydrogenases. This conclusion is consistent with the previous K-edge report, which shows at most one electron reduction from Ni–A to Ni–R [21]. In contrast to the high spin hydrogenases, the native *C. thermoaceticum* CO-dehydrogenase shows a clear low spin Ni^{II} spectrum. Preliminary results using a 15-eV resolution STJ detector and using the new ALS beamline 4.0.2 with a 0.2 eV energy resolution show a great promise for future biological L-edge spectroscopy.

Acknowledgements

The authors would like to thank Dr. Frank de Groot for many valuable discussions on theoretical calculation of the Ni L-edge spectra, Dr. C. Y. Ralston for her initial work related to the project, Prof. R. L. Smith for providing the silicon nitride membranes, Dr. R. M. Jones for his contribution in the cap design, Prof. M. W. W. Adams for *P. furiosus* hydrogenase, Prof. S. W. Ragsdale for *C. thermoaceticum* CODH, Prof. H. B. Gray for Ni-azurin, and Dr. A. T. Young and Dr. E. Arenholz for their support in the new ALS beamline 4.0.2. This work was supported by the Department of Energy, Office of Biological and Environmental Research and the National Institutes of Health grant GM-44380 (for SPC). The Stanford Synchrotron Radiation Laboratory and the Advanced Light Source are supported by the Department of Energy, Office of Basic Energy Sciences.

References

[1] J.R. Lancaster, The Bioinorganic Chemistry of Nickel, VCH, New York, 1988.
[2] S.P.J. Albracht, Biochim. Biophys. Acta-Bioenergetics 1188 (1994) 167–204.
[3] J.C. Fontecilla-Camps, Structure and Bonding 91 (1998) 2–30.
[4] A.L. de Lacey, E.C. Hatchikian, A. Volbeda, M. Frey, J.C. Fontecilla-Camps, V.M. Fernandez, J. Am. Chem. Soc. 119 (1997) 7181–7189.
[5] J.W. van der Zwaan, S.P.J. Albracht, R.D. Fontijn, E.C. Slater, FEBS Lett. 179 (1985) 271.
[6] R. Cammack, K.K. Rao, J. Serra, M.J. Llama, Biochimie 68 (1986) 93.
[7] J.J.G. Moura, M. Teixeira, I. Moura, Pure. Appl. Chem. 61 (1989) 915.
[8] C. Bagyinka, J.P. Whitehead, M.J. Maroney, J. Am. Chem. Soc. 115 (1993) 3576–3585.
[9] H.-X. Wang, G. Peng, L.M. Miller et al., J. Am. Chem. Soc. 119 (1997) 4921–4928.

[10] F.M.F. de Groot, J.C. Fuggle, B.T. Thole, G.A. Sawatzky, Phys. Rev. B 42 (1990) 5459–5468.
[11] S.P. Cramer, C.Y. Ralston, H.-X. Wang, C. Bryant, J. Electron Spectroscopy 86 (1997) 175–183.
[12] S.P. Cramer, J. Chen, S.J. George et al., Nucl. Instrum. Methods A 319 (1992) 285–289.
[13] G. van der Laan, J. Zaanen, G.A. Sawatzky, R. Karnatak, J.-M. Esteva, Phys. Rev. B 33 (1986) 4253–4263.
[14] L.J. Terminello, G.D. Waddill, J.G. Tobin, Nucl. Instrum. Methods A A319 (1992) 271–276.
[15] Z. Hussain, W.R.A. Huff, S.A. Keller et al., J. Electron Spectroscopy 80 (1996) 401–404.
[16] H.-X. Wang, C.Y. Ralston, D.S. Patil et al., J. Am. Chem. Soc. (2000) in press.
[17] C.Y. Ralston, H.-X. Wang, S.W. Ragsdale et al., J. Am. Chem. Soc. (2000) in press.
[18] H.-X. Wang, P. Ge, C.G. Riodan et al., J. Phys. Chem. B 102 (1998) 8343–8346.
[19] B.T. Thole, G. van der Laan, Phys. Rev. B 38 (1988) 3158–3171.
[20] J. van Elp, G. Peng, B.G. Searle et al., J. Am. Chem. Soc. 116 (1994) 1918–1923.
[21] Z.J. Gu, J. Dong, C.B. Allan et al., J. Am. Chem. Soc. 118 (1996) 11155–11165.
[22] J. Stohr, J. Electron Spectroscopy 75 (1995) 253–272.
[23] G. van der Laan, B.T. Thole, G.A. Sawatzky, M. Verdaguer, Phys. Rev. B 37 (1988) 6587–6589.
[24] C.P. Wang, R. Franco, J.J.G. Moura, I. Moura, E.P. Day, J. Bio. Chem. 267 (1992) 7378–7380.
[25] F. Dole, A. Fournel, V. Magro, E.C. Hatchikian, P. Bertrand, B. Guigliarelli, Biochemistry 36 (1997) 7847–7854.
[26] P. Amara, A. Volbeda, J.C. Fontecilla-Camps, M.J. Field, J. Am. Chem. Soc. 121 (1999) 4468–4477.
[27] E. Garcin, X. Vernede, E.C. Hatchikian, A. Volbeda, M. Frey, J.C. Fontecilla-Camps, Structure with Folding and Design 5 (1999) 557–566.
[28] J.Q. Xia, J. Dong, S.K. Wang, R.A. Scott, P.A. Lindahl, J. Am. Chem. Soc. 117 (1995) 7065–7070.
[29] S.W. Ragsdale, M. Kumar, Chem. Rev. 96 (1996) 2515–2539.
[30] S. Friedrich, L. Hiller, M. Frank et al., J. Electron Spectrosc. 103 (1999) 891–896.
[31] S. Friedrich, T.B. Le Graud, L.J. Hiller et al., IEEE Trans. Appl. Superconductivity 9 (1999) 3330–3333.